THE JOURNAL OF BIOLOGICAL CHEMISTRY VOL. 286, NO. 34, pp. 29748–29757, August 26, 2011

Crystal Structure of the E2 Domain of Amyloid Precursor Protein-like Protein 1 in Complex with Sucrose Octasulfate*[S]

Received for publication, January 7, 2011, and in revised form, June 6, 2011 Published, JBC Papers in Press, June 29, 2011, DOI 10.1074/jbc.M111.219659

Yi Xue[1], **Sangwon Lee**[1], **Yongcheng Wang**[2], **and Ya Ha**[3]

From the Department of Pharmacology, Yale School of Medicine, New Haven, Connecticut 06520

Missense mutations in the amyloid precursor protein (APP) gene can cause familial Alzheimer disease. It is thought that APP and APP-like proteins (APLPs) may play a role in adhesion and signal transduction because their ectodomains interact with components of the extracellular matrix. Heparin binding induces dimerization of APP and APLPs. To help explain how these proteins interact with heparin, we have determined the crystal structure of the E2 domain of APLP1 in complex with sucrose octasulfate (SOS). A total of three SOS molecules are bound to the E2 dimer. Two SOSs are bound inside a narrow intersubdomain groove, and the third SOS is bound near the two-fold axis of the protein. Mutational analyses show that most residues interacting with SOS also contribute to heparin binding, although in varying degrees; a deep pocket, defined by His-376, Lys-422, and Arg-429, and an interfacial site between Lys-314 and its symmetry mate are most important in the binding of the negatively charged polysaccharide. Comparison with a lower resolution APP structure shows that all key heparin binding residues are conserved and identically positioned, suggesting that APLP1 and APP may bind heparin similarly. In transfected HEK-293 cells, mutating residues responsible for heparin binding causes little change in the proteolysis of APP by the secretases. However, mutating a pair of conserved basic residues (equivalent to Arg-414 and Arg-415 of APLP1) immediately adjacent to the heparin binding site affects both the maturation and the processing of APP.

Since the discovery of missense mutations in the gene coding for amyloid precursor protein (APP)[4] 20 years ago (*e.g.* Refs. 1 and 2), now more than 20 APP mutations have been documented that cause familial Alzheimer disease.[5] APP is normally processed by β- and γ-secretases to give rise to a small peptide called Aβ (4). Because the senile plaque, of which Aβ is the major component (5), is one of the defining pathological features of Alzheimer disease, it has been hypothesized that Aβ is neurotoxic and can trigger biochemical changes in the brain that eventually lead to Alzheimer disease at old age (6). The disease-causing mutations in APP are all clustered around the Aβ region and appear to affect either the metabolism or the aggregation of Aβ (7).

APP and other members of its family (in mammals these include APLP1 and APLP2) are type I membrane proteins (8–10). The functions of APP and APLPs are not well understood. Mice lacking individual members of the family are viable and fertile (11–13). Only animals with double APP/APLP2 or APLP1/APLP2 knockouts or the triple knockouts show early postnatal lethality (12–14). The mice lacking APP/APLP2 seem to have defects in neuromuscular synapses (15), whereas the triple knock-out animals exhibit a high incidence of neuronal ectopia and other cranial abnormalities (14). These phenotypes could be related to the proposed function of APP family proteins in cell adhesion and signaling (16–18). At the cellular level, a subpopulation of APP molecules is localized to the plasma membrane, where they interact directly with components of the extracellular matrix (17). The large ectodomain of APP, which contains two heparin binding sites (19), can also be released from the membrane by proteolysis. The soluble ectodomain possesses growth-promoting activities and is often bound to the heparan sulfate (HS) present in the extracellular matrix and in circulation (20–22). Heparin and HS binding induces dimerization of APP and APLPs (23–26).

Because heparin modifies the aggregation and toxic properties of Aβ (27–29), there are interests in the medical field to use heparin as a therapeutic agent to treat Alzheimer disease (*e.g.* Ref. 27). Besides their direct interactions with Aβ, heparin and HS were also known to affect Aβ production itself (30–33). Some of the effects of heparin on Aβ production in cell cultures were thought to be due to its binding to β-secretase, which resulted in inhibition of the protease (33). Whether the binding of heparin and HS to APP might also influence the proteolytic processing of the precursor has not been studied before.

To help determine how APP family proteins interact with heparin and HS, we have solved the crystal structure of the E2 domain of APLP1 in complex with sucrose octasulfate (SOS) (see Fig. 1*A*). The E2 domain contains the higher affinity heparin binding site (19). Unlike the situation in a previous study (34), the ligand, as well as the protein side chains that interacted with it, has now been clearly defined in the electron density map. The crystal structure, combined with site-directed

* This work was supported, in whole or in part, by National Institutes of Health Grant GM077547 (to Y. H.).

[S] The on-line version of this article (available at http://www.jbc.org) contains supplemental Figs. S1–S3.

The atomic coordinates and structure factors (codes 3Q7L and 3Q7G) have been deposited in the Protein Data Bank, Research Collaboratory for Structural Bioinformatics, Rutgers University, New Brunswick, NJ (http://www.rcsb.org/).

[1] Both authors contributed equally to this work.

[2] Present address: Monsanto Company, 700 Chesterfield Pkwy. W., Chesterfield, MO 63017.

[3] To whom correspondence should be addressed: Dept. of Pharmacology, Yale School of Medicine, 333 Cedar St., New Haven, Connecticut 06520. Tel.: 203-785-7530; Fax: 203-785-7670; E-mail: ya.ha@yale.edu.

[4] The abbreviations used are: APP, amyloid precursor protein; APLP, APP-like protein; Aβ, amyloid-β; HS, heparan sulfate; SOS, sucrose octasulfate; CTF, C-terminal fragment; Bis-Tris, 2-(bis(2-hydroxyethyl)amino)-2-(hydroxymethyl)propane-1,3-diol; Tricine, *N*-[2-hydroxy-1,1-bis(hydroxymethyl)ethyl]glycine.

[5] J. Hardy and R. Crook, unpublished data.

mutagenesis, permitted the identification of all key heparin binding residues in the E2 domain. We also studied the effects of mutating some of these residues on the proteolytic processing of APP in cultured human embryonic kidney (HEK)-293 cells.

EXPERIMENTAL PROCEDURES

Reagents—The sodium salt of SOS was obtained from Toronto Research Chemicals Inc. The heparin disaccharides were obtained from Sigma-Aldrich (H9267 and H9392). Heparin was purchased from Santa Cruz Biotechnology (sc-203075).

Plasmid Construction and Protein Preparation—The $APLP1_{285-494}$ fragment was amplified by PCR from human APLP1 cDNA (Open Biosystems, MHS1010-74392) and subcloned into pET28a vector (Novagen). The recombinant protein was expressed in BL21-Gold(DE3) cells (Agilent Technologies) in LB medium. The cells were induced with 0.5 mM isopropyl-1-thio-β-D-galactopyranoside at A_{600} 0.5 and were left to grow overnight at room temperature. The cells were harvested and resuspended in the lysis buffer of 20 mM sodium phosphate, pH 7.8, 0.5 M NaCl, and EDTA-free protease inhibitor mixture (Roche Applied Science). The cells were lysed by freeze and thaw in the presence of lysozyme. The cell lysate was applied to a Talon metal affinity column (Clontech), and the recombinant protein was eluted with 200 mM imidazole. The N-terminal hexahistidine tag was removed by thrombin. The protein without His tag was concentrated and further purified on a Superdex S-200 column (GE Healthcare) in a buffer containing 20 mM HEPES, pH 7.5, 0.5 M NaCl, and 5% glycerol. The peak fraction was pooled and concentrated to 10 mg/ml and stored at −20 °C. All mutants were generated using the QuikChange® site-directed mutagenesis kit. They were expressed and purified similarly.

Crystallization and Structural Determination—$APLP1_{285-494}$ was initially crystallized by the hanging-drop method. The reservoir solution contained 25% PEG 3350, 0.1 M Bis-Tris, pH 6.5, 0.2 M Li_2SO_4, and 25 mM ATP. Rod-shaped crystals usually showed up overnight and grew to a maximum size of 0.3 × 0.05 × 0.05 mm after 3 days. The crystals were sensitive to exposures to the air and could only be cryo-preserved by Paratone oil with a low success rate, which greatly hindered the soaking experiment. To overcome this problem, we tried other crystallization and cryo-protection methods. The microbatch crystallization method, which allowed all soaking and cryo-preserving steps to be performed under oil, was found to be most suitable for our purpose. We also found that adding glycerol to the mother liquor increased the success rate of cryo-protection. In summary, the 1:1 mixture of protein and crystallization solutions (25% PEG 3350, 0.1 M Bis-Tris, pH 6.5, 0.2 M Li_2SO_4, 25 mM ATP) was pipetted into the 72-well microbatch plate immersed with Al's oil (a 1:1 mixture of silicone oil and paraffin oil, Hampton Research). After overnight incubation, streak-seeding was performed to expedite crystallization. After seeding, crystals usually grew to maximum size in 24 h and were ready for soaking. SOS was dissolved in the crystallization solution and added to the drops to reach final concentrations of 1, 5, 10, 15, 20, and 50 mM. After overnight soaking, the crystals were cryo-preserved by stepwise exchange of the mother liquor with a crystallization solution supplemented with 25% glycerol. The crystals were flash-cooled in liquid nitrogen. We also tried to soak the heparin disaccharides into the crystal using a similar protocol. To minimize the potential competition of the sulfate ions and ATP present in the crystallization solution with the ligand, we also lowered the concentrations of Li_2SO_4 and ATP in the artificial mother liquor. Although ATP was not essential, 20 mM Li_2SO_4 was required to maintain the diffraction quality of the crystals; however, even at 20 mM Li_2SO_4 and without ATP, the heparin disaccharides still failed to bind to the protein. X-ray diffraction data were collected from beamlines X25 and X29 at the National Synchrotron Light Source (NSLS) and processed by HKL2000 (35). The packing of the PEG crystal form was similar to that of a previous crystal form obtained from phosphate salts (23). For the apo-structure (and those treated with heparin disaccharides), rigid body refinement of the relative positions of the two subdomains by CNS (36) followed by a few steps of positional and temperature factor refinement was sufficient to lower the *R* from 48% to about 29% (R_{free} 33%). For the SOS complex, however, the *R* after similar refinement remained high (*R* 32%; R_{free} 36%). After manual adjustment of the protein model using O (37) based on $2F_o - F_c$ and $F_o - F_c$ maps, the *R*-factor could be lowered to 29%. The improvement in the accuracy of the phase finally rendered the A site (the SOS binding site in the A chain) interpretable. The streak of positive peaks lying across helix αD in the difference Fourier map, initially thought to be due to another bound SOS molecule, now appeared to correspond to a segment of polypeptide chain near the C terminus of the protein, which was disordered in the apo-structure. After adding the missing segment to the protein model (residues 487–494 of the A chain; see Fig. 1*B*, *red*), it became clear that the remaining densities at the A site corresponded a single SOS molecule. Incorporation of the SOS molecules to the model using coot (38) caused R_{free} to immediately drop another 1.2%, which further confirmed the presence of SOS at the binding sites. Further refinements were carried out using refmac5 (39). Crystallographic statistics are available in Table 1 .

Heparin Binding Assay—After exchanging into a buffer of 10 mM sodium phosphate/acetate, pH 7.5, the protein solutions were loaded onto the 1-ml HiTrap heparin column (GE Healthcare) and eluted with a linear salt gradient (0–2 M NaCl). The eluting NaCl concentrations were calculated based on the measured conductivity.

APP Processing in Transfected HEK-293 Cells—HEK-293 cells were cultured in Dulbecco's modified Eagle's medium (DMEM) supplemented with 4.5 g/liter glucose, 10% fetal bovine serum, 100 units/ml penicillin, and 100 μg/ml streptomycin on a 6-well tissue culture dish. The human APP_{751} sequence was subcloned into pcDNA3.1(−) expression vector (Invitrogen) with an engineered C-terminal Myc tag. After reaching 70–80% confluency, the cells were transfected with the plasmid (1.5 μg of DNA/well) using Lipofectamine™ 2000 (5 μl/well) (Invitrogen). After 36 h, the transfected cells were harvested and lysed in a lysis buffer containing 10 mM Tris, pH 7.4, 150 mM NaCl, 0.1% sodium deoxycholate, 1% Nonidet P-40, and the Complete protease inhibitor mixture (Roche Applied Science). The cell lysates were resolved by

TABLE 1
Crystallographic statistics
APLP1 was crystallized in space group $P2_12_12_1$.

	Apo-APLP1	APLP1-SOS
Data collection		
Cell dimensions (Å)	$a = 73.0$, $b = 83.0$, $c = 89.2$	$a = 73.5$, $b = 82.2$, $c = 89.9$
Wavelength (Å)	1.071	1.075
Resolution[a] (Å)	40.0-2.2 (2.28-2.20)	40.0-2.3 (2.38-2.30)
Observed reflections	205,043	339,192
Unique reflections	28,355	24,869
Redundancy	7.2	13.6
Completeness[a] (%)	99.9 (100.0)	99.7 (99.4)
$<I/\sigma>^a$	13.2	13.6
$R_{merge}{}^{a,b}$	0.054 (0.389)	0.084 (0.491)
Refinement		
Resolution (Å)	40.0-2.2	40.0-2.3
$R_{work}/R_{free}{}^c$	0.216/0.256	0.217/0.261
Number of atoms		
Protein	2,978	3,040
Sulfate ion	10	
SOS		165
Water	283	162
***B*-factors**		
Protein	50	50
Sulfate ion	65	
SOS (A, B, C)		114, 97, 131
Water	57	57
r.m.s. deviations[d]		
Bond lengths (Å)	0.006	0.012
Bond angle (°)	1.04	1.47

[a] Highest resolution shell is shown in parentheses.
[b] $R_{merge} = \sum| I_i - \langle I \rangle |/\sum I_i$.
[c] $R_{work} = \sum| F_o - F_c |/\sum F_o$. R_{free} is the cross-validation *R*-factor for the test set of reflections (10% of the total) omitted in model refinement.
[d] r.m.s., root mean square.

Novex 16% Tricine gels (Invitrogen) and visualized by Western blot using mouse anti-c-Myc antibody (1:500) (Invitrogen) and goat anti-mouse alkaline phosphatase-conjugated secondary antibody (1:5,000) (Novagen). The mutants were generated using the QuikChange® site-directed mutagenesis kit and similarly expressed in HEK-293 cells.

RESULTS

Overall Structure of the Complex—The new crystallization condition, which used PEG instead of phosphate salts as precipitant, was ideal for the heparin soaking experiment because the binding of heparin to E2 was inhibited at high salt concentrations. Direct soaking with a longer heparin compound unfortunately disrupted the crystal lattice. We therefore resorted to the shorter heparin disaccharides and SOS, a disaccharide that, like heparin, is heavily substituted with sulfate groups (Fig. 1*B*). Diffraction data were collected from many crystals that had been soaked either in blank solutions or in solutions containing different concentrations of the disaccharides. Difference Fourier analysis showed that only SOS bound to the protein in the crystal. In the apo-structure, a strong peak (~8 σ) was observed between Lys-422, Arg-425, and Arg-429, which probably corresponded to a bound sulfate ion from the crystallization solution (which contained 200 mM Li_2SO_4) and was similar in appearance to the bound phosphate ion in a previously solved structure (Fig. 1*C*). The sulfate peak was not affected by the soaking of two heparin disaccharides (map not shown). In the difference map of the SOS complex, the strong sulfate peak disappeared, and a cluster of new peaks (~6 σ), which contained an elongated central peak and eight peaks around it, appeared in a nearby groove between the two subdomains of the B chain of the E2 dimer (the B site; Fig. 1*D*). Later refinement showed that the peripheral peaks corresponded to the eight sulfate groups of SOS. The difference density features in chain A (the A site) were more complex initially due to rearrangements in the protein structure (see below). The difference map also suggested that there was a third and weaker SOS binding site (the C site) at the interface between the two protein protomers (Fig. 1*B*).

Binding of SOS to the A and B Sites—The SOSs bound at the A and B sites were clearly defined in the electron density map (supplemental Fig. S1). Although the ligand was bound to the protein differently, the backbone of the disaccharides had similar conformations (supplemental Fig. S2*A*); the rotational angles around the two single bonds of the $\alpha(1\rightarrow2)$ glycosidic linkage were similar so that the two sugar rings were superposable simultaneously. The SOS bound at the interfacial C site also appeared to adopt this conformation, although we were less certain about its modeling due to poor electron densities (supplemental Figs. S1*C* and S2*B*). The conformation of the sugar observed here had been observed before in other crystallographic studies of protein-SOS complexes (for example, see Ref. 40) (supplemental Fig. S2*C*).

The binding of SOS to the A site displaced the sulfate ion bound to Lys-422, Arg-425, and Arg-429 in the apo-structure (Fig. 2*A*). The sulfate group connected to the C2 atom of the glucose (Glc) moiety of SOS now occupied a nearby site and was hydrogen-bonded to Arg-425 and Arg-429. The same sulfate group also formed a hydrogen bond with His-426, whose side chain rotated 60° around the $C\alpha$-$C\beta$ bond to move into the binding site. The sulfate group on C3 of the glucose was hydrogen-bonded to His-489, which was part of the C-terminal segment that was disordered in the apo-structure (Fig. 2*C*). The sulfate on glucose C4 was hydrogen-bonded to Arg-418, whose side chain was also disordered in the apo-structure. The sulfate on glucose C6 was hydrogen-bonded to Arg-418 and Lys-422. The fructose (Fru) moiety of SOS was raised to interact with residues from the N-terminal subdomain of E2. The sulfate on fructose C1 was hydrogen-bonded to His-426 and interacted with Lys-422 and the backbone amide group of His-307 via bridging water molecules. The sulfate on fructose C4 formed a hydrogen bond with Ser-305, and the sulfate on fructose C6 was hydrogen-bonded to Gln-387 and Lys-422. The sulfate on fructose C3 did not appear to engage in any direct interactions with the protein.

SOS was bound to the B site in a completely different mode (Fig. 2*B*). The disaccharide appeared to be flipped by 90°, and most of the interactions with the protein were mediated now through sulfate groups on the fructose moiety. The sulfate group on fructose C1 was hydrogen-bonded to Lys-422* and Arg-429* (the asterisk denotes the B-chain). The sulfate group on fructose C3 penetrated deep into the space between the two subdomains and formed a hydrogen bond with His-376*. The sulfate on fructose C3 also interacted with His-307* via a water molecule. The sulfate on fructose C4 interacted with the backbone amide of His-307* via a water molecule. The ester oxygen on fructose C6 was hydrogen-bonded to Lys-422*. The ring oxygen of the fructose also

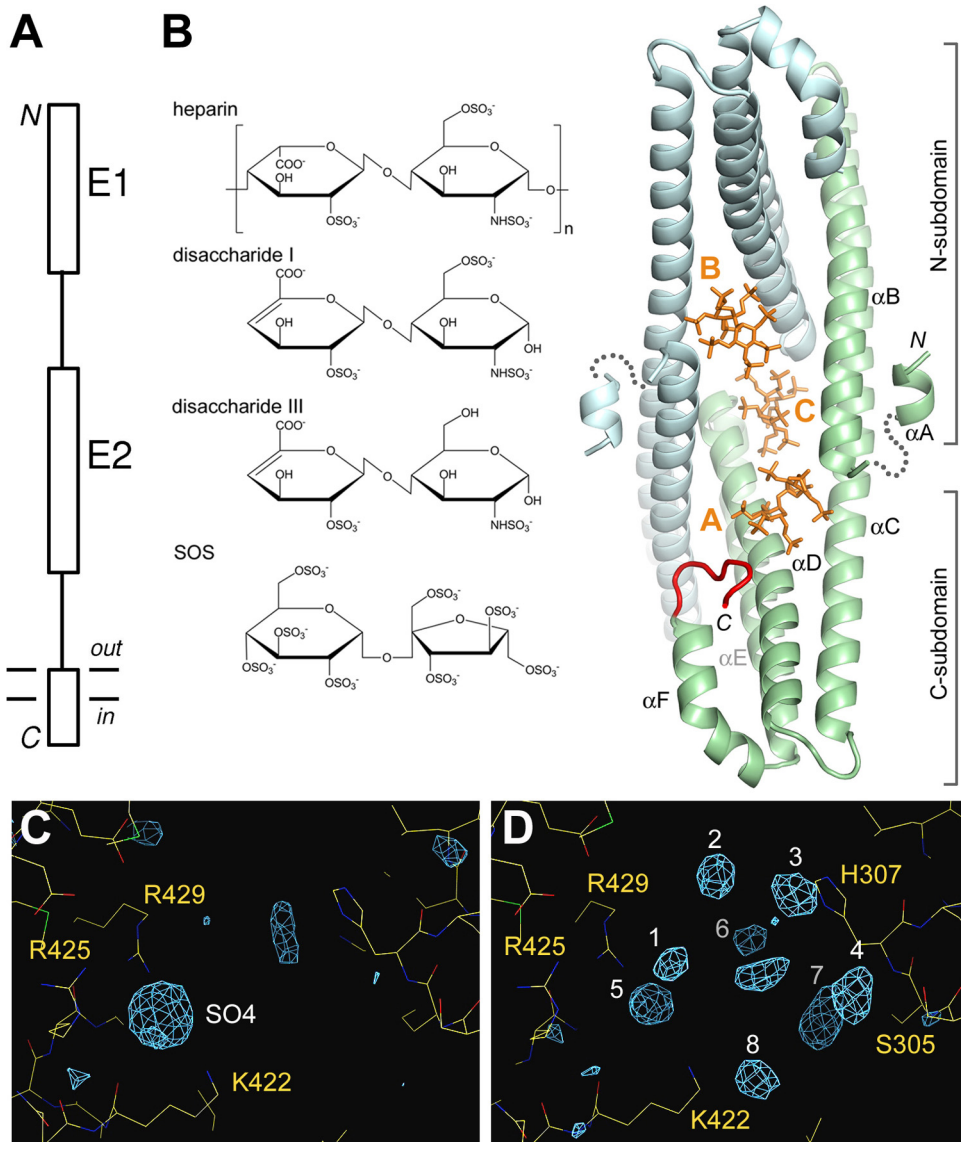

FIGURE 1. **Overall structure of the complex.** *A*, a cartoon representation of the domain structure of APLP1. The *two horizontal lines* represent the boundaries of the membrane. *B*, the chemical structures of heparin, heparin disaccharides, SOS, and the crystal structure of the E2-SOS complex. The two protein protomers (A and B chains) are shown in *green* and *blue*, respectively. The N-terminal helices αA have been domain-swapped with neighboring molecules and modeled back to their original positions (26). The helices (αA–αF) and subdomains (N, C) in the A chain are labeled. The C terminus of the A chain that had become ordered is shown in *red*. The bound SOS molecules is shown in *orange*. This illustration and those in Figs. 2–5 were generated by PyMOL. *C*, difference Fourier map showing a bound sulfate ion in the apo-structure (the B chain). *D*, difference map of the SOS-soaked crystal revealing a cluster of positive densities at a nearby site. *Peaks 1–8* correspond to the sulfate groups attached to the C2, C3, C4, and C6 of the glucose moiety and C1, C3, C4, and C6 of the fructose moiety of SOS, respectively. The difference maps in *C* and *D* are both contoured at 3.5 σ levels.

appeared to form a hydrogen bond with Lys-422*. The glucose moiety of SOS made only two direct interactions with the protein (between the sulfate group on C2 and Arg-429* and between the sulfate on C6 and Ser-305*). All other interactions were mediated through water molecules.

The non-crystallographic two-fold symmetry, which related the A and B sites, was not exact. In the apo-structure, it was already apparent that the A site was narrower than the B site as the result of a small "movement" of the αB helix. The binding of SOS to the A site caused αB to move further inwards (see below). Therefore, to accommodate SOS in a similar orientation at the wider B site would require a bigger movement in αB, which seemed to be restricted by crystal packing. On the other hand, the binding mode of SOS observed at the B site would cause steric clashes inside the narrower A site.

Binding of SOS to the Interfacial C Site—Difference Fourier analysis suggested that there might be a third SOS molecule bound to the protein near the two-fold axis (Fig. 1*B*). Fig. 3*A* showed the features of the difference map in this region. Among the peaks shown, two (*peaks 6* and *7*) had intensities around 7 σ, and three (*peaks 1*, *4*, and *5*) had intensities around 5 σ. The intensities of the peaks and their proximity to each other were consistent with the possibility that they corresponded to sulfate groups on the same SOS molecule. The model shown in Fig. 3*B* represented the best fit that we could achieve in modeling SOS into the difference densities. The broken electron densities in the final $2F_o - F_c$

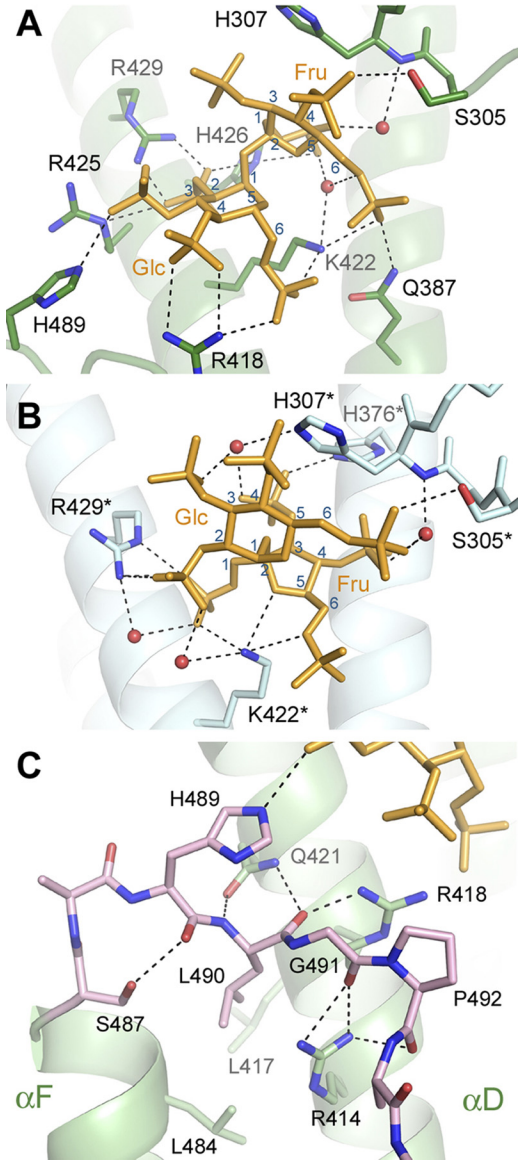

FIGURE 2. **Binding of SOS to the A and B sites.** *A*, the A site. SOS is shown in *orange*. The carbon atoms (C1–C6) of the glucose and fructose moieties are labeled. Water molecules are shown as *red spheres*. *Dashed lines* represent hydrogen bonds. *B*, the B site. Residues in the B chain are indicated by the *. *C*, interactions between the C terminus and the αD helix of the protein. The C-terminal fragment of the A chain that had become ordered in the crystal is shown in *pink*. SOS is shown in *orange*. *Dashed lines* represent hydrogen bonds.

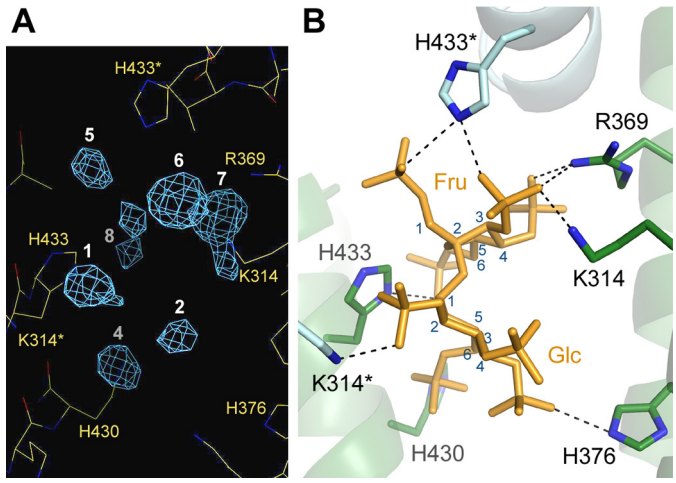

FIGURE 3. **Binding of SOS to the interfacial C site.** *A*, difference Fourier map (contoured at 3.5 σ levels) reveals a cluster of positive peaks near the two-fold axis of the protein. *B*, a model of SOS bound at the C site. With the exception of the sulfate group attached to the C4 of glucose, all other sulfate groups were well defined in the difference map (*peaks 1*, *2*, and *4*–*8* in *A*).

map suggested that the backbone of the sugar was probably flexible.

As evident from the distribution of the peaks in the difference map, the binding of SOS to the interfacial C site was highly asymmetrical. The center of the mass of the ligand was shifted toward the A chain and away from the two-fold axis (between the two His-433 residues in Fig. 3*A*). In our model, only two residues from the B chain made contacts with the ligand (Fig. 3*B*); Lys-314* formed a hydrogen bond with the sulfate group on glucose C2, and His-433* was hydrogen-bonded to the sulfate groups on fructose C1 and C3. In contrast, five residues from the A chain interacted with the ligand. Lys-314 and Arg-369 were hydrogen-bonded to the sulfate groups on fructose C3 and C4. His-376 seemed to interact with the sulfate on glucose C4 (although this sulfate group was not well defined in the electron density map). His-430 was hydrogen-bonded to the sulfate on glucose C6, and His-433 was hydrogen-bonded to the sulfate group on fructose C6. The interactions between SOS and the protein at the C site were not as extensive as those in the A and B sites. The reason that the sugar was bound mostly to the A chain and in one orientation, instead of to the symmetry-related site in the B chain, seemed to be due to a potential clash with the SOS molecule bound at the B site; the sulfate group on fructose C3 of the B site SOS, which was also hydrogen-bonded to His-376* (Fig. 2*B*), would be too close to the sulfate group on glucose C4 of the C site SOS if the latter was bound to the B-chain.

Neither SOS nor heparin had an intrinsic two-fold symmetry. Therefore, the inability of the interfacial C site to simultaneously accommodate two SOS molecules (or heparin disaccharides) seemed to dictate that the binding of ligand to the E2 dimer had to be asymmetrical.

Conformational Changes Induced by SOS Binding—The binding of SOS to the protein caused little structural change in the B chain. The A chain, however, showed many subtle movements (supplemental Fig. S3*A*). The αB helix shifted 0.7 Å toward the C-terminal subdomain to position Ser-305 and His-307 closer to the ligand. The middle portion of αC near His-376 moved back slightly to generate room for the A site SOS. The αD helix also bent back after His-433 to accommodate the C site SOS (the side chain of His-433 moved by about 1.5 Å). Inside the A site binding pocket (Fig. 2*A*), the side chain of Arg-418 had become ordered. The side chains of Lys-422 and His-426 also changed conformation to better interact with the ligand.

A segment of the polypeptide at the C terminus of the A chain (residues 487–494) had become ordered (Fig. 1*B*, *red*; supplemental Fig. S3*B*). His-489 from this segment formed a hydrogen bond with the A site SOS. The ordering of the peptide segment was probably responsible for the 1.2 Å movement of the C-terminal helix αF, which had now become more similar in structure to its B chain counterpart. This similarity suggested

TABLE 2
Summary of mutant data

The affinity for heparin was expressed empirically as the molar salt concentration required for eluting the protein from a heparin column. The percentages of the salt concentration relative to the wild-type (WT) value are shown in parentheses.

	Mutation	[NaCl]
		M (%)
	WT	0.70 (100)
N-terminal subdomain (A/B)	S305A	0.46 (66)
	H307A	0.45 (65)
	H376A	0.41 (58)
C-terminal subdomain (A/B)	Q387A	0.66 (95)
	R418A	0.48 (69)
	K422A	0.22 (32)
	R425A	0.50 (72)
	H426A	0.63 (90)
	R429A[a]	0.38 (54)
Dimeric interface (C)	K314A	0.31 (44)
	R369A[a]	0.53 (76)
	H430A	0.55 (79)
	H433A[a]	0.50 (72)
C-terminal peptide	R414A	0.58 (83)
	Q421A	0.74 (107)
	H489A	0.68 (98)

[a] These three mutants had been described by Lee *et al.* (26).

that the new position of αF, and possibly the ordered C-terminal segment, might represent the natural conformation of the protein in solution, which was not influenced by crystal packing and should therefore be more symmetrical.

The ordered C terminus of the protein folded back to interact mostly with residues on the αD helix (Fig. 2*C*). The side chain of Gln-421 was simultaneously hydrogen-bonded to the backbone amide and carbonyl groups of Leu-490; Arg-418 formed a hydrogen bond with the carbonyl oxygen of Leu-490 also, whereas Arg-414 was hydrogen-bonded to the carbonyl group of Gly-491. These interactions helped keep the main chain of the peptide in an extended conformation. Because Arg-414, Arg-418, and Gln-421 were all highly conserved, one might predict that the peptide binding site was a common feature for all APP family proteins. The folded back peptide was further stabilized by hydrophobic interactions between Leu-490 and the conserved Leu-417 and Leu-484 (from αF). The turns at the two ends of the peptide segment were stabilized by hydrogen bonds between Ser-487 and the carbonyl oxygen of His-489 and between Arg-414 and the carbonyl oxygen of Pro-492.

Mutagenesis Mapping of the Heparin Binding Site—The residues that interacted with SOS (and the C-terminal peptide; see below) were tested for their role in heparin binding by site-directed mutagenesis. In Table 2, we have grouped them in four categories based on their positions in the three-dimensional structure.

Residues from the N-terminal subdomain, including Ser-305, His-307, and His-376, constituted the right-hand and upper side of the binding pocket at the A/B sites. Although Ser-305 contributed only one hydrogen bond to SOS binding, its substitution by an alanine reduced the salt concentration required to elute the protein from the heparin column by 34%. The side chain of His-307 interacted with two sulfate groups through a water molecule at the B site, and its mutation reduced the elution salt concentration by 35%. His-376 was located near the bottom of the binding pocket and contributed only one hydrogen bond to SOS binding at the B site. However, its mutation produced a larger effect (reducing the salt concentration by 42%). These results indicated that although residues from the N-terminal subdomain did not appear to form many interactions with SOS, they played important roles in heparin binding. The large contribution of His-376 to heparin binding suggested that the polysaccharide must be bound deep inside the groove between the two subdomains (Fig. 4*A*).

The left-hand side of the binding pocket at the A/B sites was composed mostly of residues from αD in the C-terminal subdomain. Here the mutation of Lys-422 reduced the salt concentration by 68%, which was the largest effect observed in this study. The side chain of Lys-422, which was not observed in the electron density maps of previously solved APP and APL-1 structures (34, 41), was at the center of the intersubdomain groove. Its positive charge and flexibility rendered it ideal for interacting with heparins. In the present structure, it was involved in at least three hydrogen-bonding interactions with SOS. The next important residue after Lys-422 was Arg-429, whose mutation reduced the salt concentration by 46%. The side chain of Arg-429 defined the left-hand side of the binding pocket directly across from His-307. It formed four hydrogen bonds with SOS at the B site. After Arg-429, mutations of Arg-418 and Arg-425 produced some moderate effects (reducing the salt concentration by 31 and 28%, respectively). The mutation of His-426, whose side chain made a rotation into the binding pocket to make two hydrogen bonds with the A site SOS, produced only a small effect (10%). Gln-387 (from αC), on the other hand, appeared to make no contribution to heparin binding.

The involvement of residues at the interfacial C site in heparin binding was confirmed by mutagenesis. Here the mutation of Lys-314 produced the second largest effect observed in our study (56%). In the SOS complex, although it only contributed one salt bridge to ligand binding, Lys-314 and its symmetry mate (Lys-314*) interacted simultaneously with the C site SOS from opposite sides of the sugar (Fig. 3*B*). Therefore, the large effect of the K314A mutation could be due to the loss of two side chains that interacted with the same heparin molecule. The mutations of Arg-369 and His-433, which were also close to the two-fold axis, affected heparin binding to lesser degrees (24 and 28%, respectively). The mutation of His-430 reduced heparin binding only moderately (20%).

The folded back C terminus of the protein did not appear to make any positive contribution to heparin binding. As shown above, His-489 was the only residue from this part of the protein that made a hydrogen bond with SOS (Fig. 2*C*). The mutation of His-489 did not change the elution salt concentration of the protein from the heparin column. The mutation of Gln-421, whose side chain helped to anchor the C terminus on αD, actually increased the affinity of the protein for heparin slightly. Taken together, these results suggested that the folded back peptide interfered with heparin binding. Arg-414 appeared to have a dual role. On the one hand, like Gln-421, it stabilized the fold-back conformation of the peptide by making three hydrogen bonds to its backbone; on the other hand, being positively charged, it could also interact favorably with heparin after the peptide had moved away. The small reduction in the elution salt

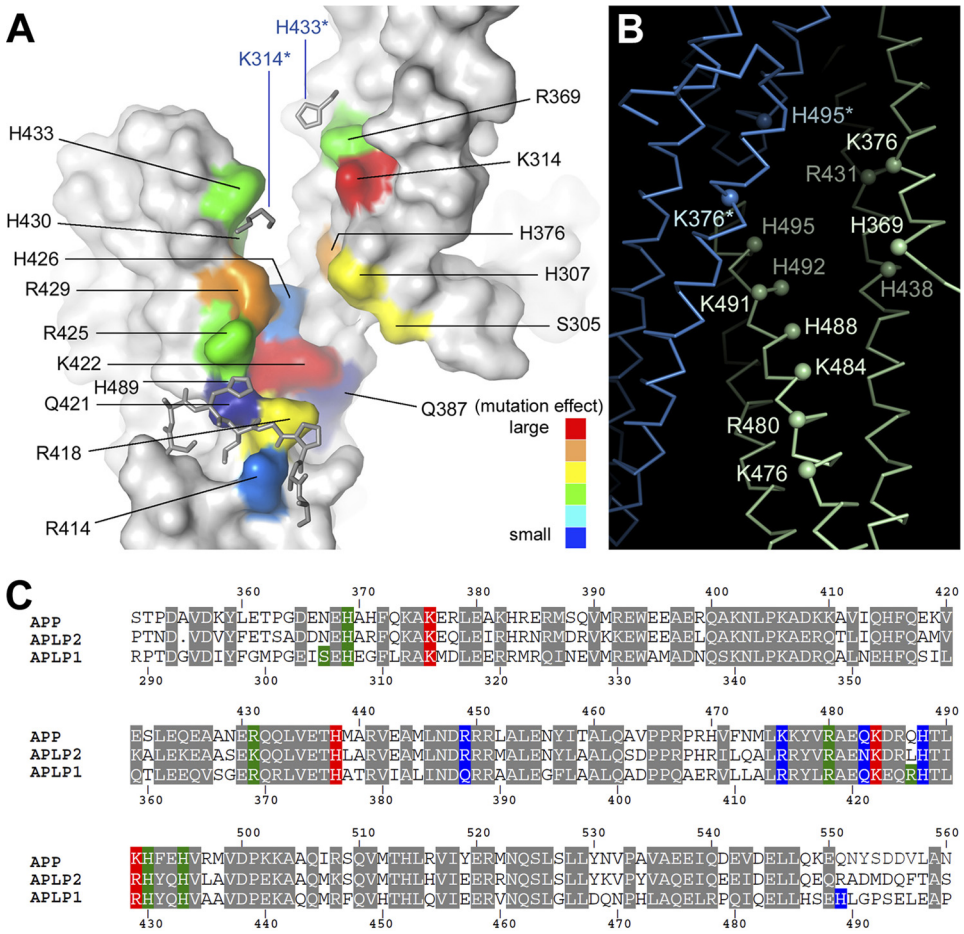

FIGURE 4. **Mutagenesis mapping of the heparin binding site.** *A*, a surface representation of the heparin binding site in the A chain (for clarity, the B chain is not shown). The folded back C-terminal fragment is shown as *sticks*. Lys-314* and His-433* from the B chain (labeled in *blue*), which probably contributed to heparin binding to the A chain, are also shown as *stick models*. The effect of the mutations on heparin binding is represented by different colors, with *red* showing the largest reduction of the salt concentration required to elute the protein from the heparin column (>50%) and *dark blue* showing no obvious reduction. *B*, the Cα trace of APP viewed from a similar angle (26). The nine conserved residues whose mutation reduced the affinity of APLP1 for heparin by more than 20% are shown as *small spheres*. The conserved Lys-476 and His-488 (equivalent to Arg-414 and His-426 of APLP1) are also shown. *C*, sequence alignment of the E2 domains of the three human APP family proteins. Conserved residues are *highlighted*. The 16 mutated APLP1 residues are highlighted in *red*, *green*, and *blue*, indicating their contributions to heparin binding (*red* being the most important).

concentration (17%) for the R414A mutant likely reflected a compromise between these two opposing effects.

The Heparin Binding Site Was Conserved—In Fig. 4*A*, the effects of the 16 single mutations on heparin binding were color-mapped onto the protein surface. Among these, 11 reduced the elution salt concentration of the protein from the heparin column by more than 20% (Fig. 4*A*, *red* to *green*). With the exceptions of Ser-305 and Arg-425, the other nine were conserved in APP and APLP2 (Fig. 4*C*, *red* and *green*). Ser-305 probably played a structural role (*e.g.* by capping the N terminus of αB, which could be substituted by Asn-367 of APP) instead of participating directly in ligand binding because it did not carry any positive charge. Arg-425 contributed only weakly to heparin binding and might be specific to APLP1.

A lower resolution crystal structure of APP had already been known (41). Although there were large differences between the APP and APLP1 structures, mostly in the angles between the two subdomains and between the two protein protomers (26), the region that was important for heparin binding remained similar (Fig. 4*B*). The conserved nine residues were similarly positioned in APP around a groove between the two subdomains and were not hindered by protein dimerization; Lys-376* and His-495* (equivalent to Lys-314* and His-433* of APLP1) from the symmetry-related molecule were also adjacent and exposed in the dimer to constitute a similar interfacial binding site.

The Effect of the Mutations on APP Processing—The complete mapping of the high affinity heparin binding site enabled us to examine whether binding of endogenous HS to the E2 domain of APP could influence APP processing. In HEK-293 and many other mammalian cell types, only a small fraction of the total pool of cellular APPs was processed by β-secretase, which generated a membrane-bound C-terminal fragment (CTF) called C99; a larger fraction of the APP pool was processed by the competing α-secretase, which produced C83 (42). C99 and C83 were further cleaved by γ-secretase to give rise to Aβ and p3, respectively (Fig. 5*A*). To help visualize various APP species in intact HEK-293 cells, we engineered a Myc tag to the C terminus of APP_{751}. Western blot analysis of the transfected cells using an anti-Myc antibody showed two sets of bands (Fig. 5*B*). The high molecular mass bands at 100 and 120 kDa corresponded to the immature and mature full-length APPs, respec-

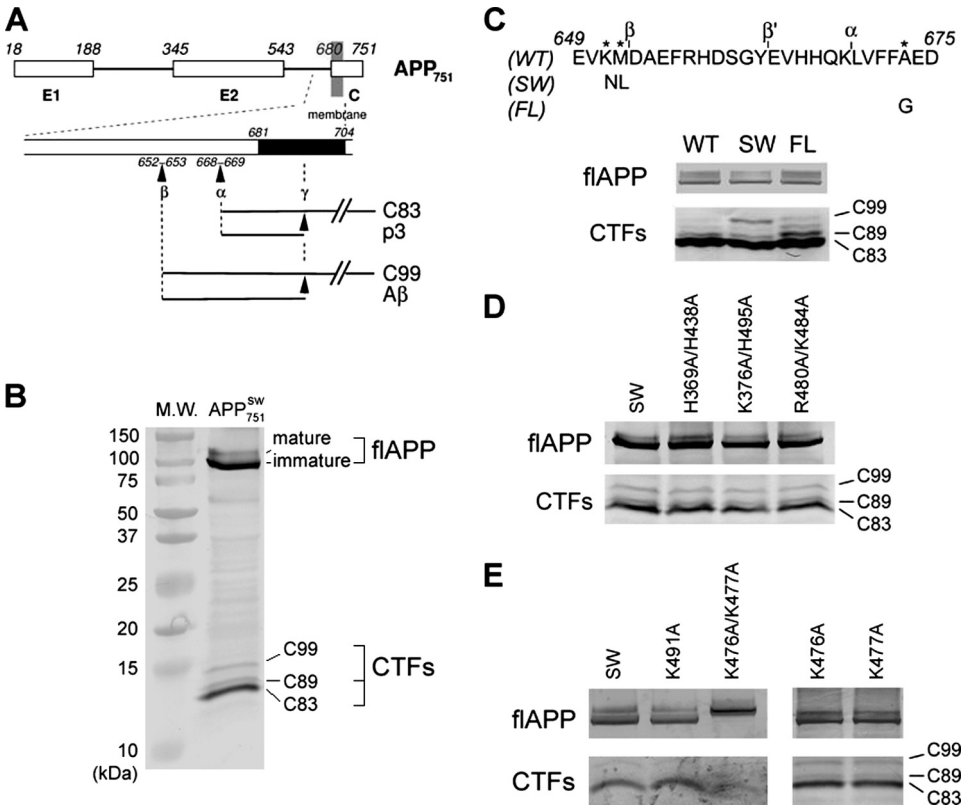

FIGURE 5. **The effect of mutations on APP processing in live HEK-293 cells.** *A*, a schematic diagram of APP_{751} and its juxtamembrane region. The *white boxes* represent the three conserved regions (E1, E2, and C), and the *black box* represents the transmembrane domain. *B*, a typical Western blot of the lysate of cells transfected with the Myc-tagged APP_{751}. Here the Swedish mutant was used to show the C99 band. *M.W.*, molecular mass markers; *flAPP*, full-length APP. *C*, the cleavage site sequence for the wild-type (WT) and the Swedish (*SW*) and Flemish (*FL*) mutants. In transfected HEK-293 cells, the C83 levels were comparable, indicating that the α-site cleavage was not significantly affected by the disease mutations. The Swedish mutation produced more C99, whereas the Flemish mutation produced not only more C99, but also more C89 and a species that migrated between them. The new CTF likely resulted from a cleavage between Phe-656 and Arg-657 (3). *D*, the heparin binding site mutations did not alter the levels of the CTFs. *E*, the K476A/K477A double mutation affected the mobility of the full-length protein and reduced the processing of APP by the secretases.

tively (42); the dark band between the 10- and 15-kDa markers was C83, the major CTF generated by α-secretase. The presence of the C-terminal Myc tag did not appear to alter the maturation and processing of APP. The effects of the well studied Swedish and Flemish disease mutations on APP processing were readily detectable by our assay (Fig. 5*C*). The Western blot showed that both mutations led to higher levels of C99 and that the Flemish mutation also increased the intensities of C89 (resulting from β'-site cleavage) and another band between C89 and C99.

We generated three double mutants inside the E2 heparin binding site (all on top of the Swedish mutation background for increased visibility of C99). The first mutant H369A/H438A eliminated two important side chains from the N-terminal subdomain (these residues corresponded to His-307 and His-376 of APLP1 in Fig. 4*A*). The second mutant K376A/H495A targeted the interfacial binding pocket (corresponding to Lys-314 and His-433 of APLP1). The third mutant R480A/K484A eliminated two positively charged side chains from the C-terminal subdomain (corresponding to Arg-418 and Lys-422 of APLP1). Western blot analysis showed that HEK-293 cells transfected with the double mutants accumulated similar levels of C83, C89, and C99 as the Swedish mutant alone (Fig. 5*D*). This result suggested that under our experimental conditions, the binding of endogenous HS to the E2 domain did not appear to affect the proteolytic processing of APP by α- and β-secretases.

Besides the three double mutants described above, we also mutated several other residues that were nearby. Like the three, most mutations (*e.g.* K491A) did not show any obvious effect in the cell culture experiment (Fig. 5*E*). The only exception was the double mutant K476A/K477A (these residues corresponded to Arg-414 and Arg-415 of APLP1). On Western blot, both immature and mature full-length APPs migrated consistently to higher molecular weights; the intensities of the CTFs were also much lower than the other mutants, suggesting greatly reduced processing by the secretases (Fig. 5*E*). Because in the APLP1-SOS crystal structure Arg-414 was involved in hydrogen bonding to the peptide backbone of the C terminus of the protein (Fig. 2*C*), we initially wondered whether the observed effect could result from a disruption of these interactions. However, mutating the equivalents of the other two residues (Arg-418 and Gln-421) that also interacted with the peptide backbone and mutating Lys-476 alone did not affect the mobilities of the full-length APP bands. Mutating Lys-477 alone also failed to produce any effect (Fig. 5*E*). Therefore, the observed differences in APP maturation and processing had to result from the simultaneous loss of both side chains of Lys-476 and Lys-477.

DISCUSSION

The E2-SOS complex structure described here was more informative than a previous study in which SOS had been soaked into the crystals of the worm homolog APL-1 (34). In the worm structure, although the sugar was also found to bind between the two subdomains, the ligand was poorly defined in the electron density map. Only the glucose moiety of SOS was weakly visible; most of the sulfate substituents and the fructose moiety were disordered. Accordingly the ligand appeared to interact with only three protein side chains (they corresponded to Ser-305, His-307, and His-426 of APLP1). The crystal structure reported here suggested that at least 10 more residues could contribute to heparin binding. Furthermore, we recently showed that heparin binding induced E2 dimerization (26). The worm protein was crystallized as monomers and did not contain the binding pocket at the dimer interface, *e.g.* between Lys-314 and its symmetry mate. Therefore, the new crystal structure appeared to be a better mimic of the $(E2)_2$-heparin complex. The mutagenesis data presented here also showed that residues located deep inside the intersubdomain groove (*e.g.* His-376) and near the two-fold symmetry axis of the protein (*e.g.* Lys-314), whose roles in ligand binding were not previously recognized, were some of the key players in heparin binding.

Three new conclusions about E2-heparin binding could be drawn from our current study. Firstly, heparin appeared to bind to two "hot spots" on the protein surface (Fig. 4*A*, *red*). The first hot spot was defined by His-376, Lys-422, and Arg-429 and coincided roughly with the A/B site of the E-SOS complex. His-376 and Arg-429 formed the opposing walls of a narrow groove between the two subdomains, whereas Lys-422 lay on the bottom of the groove near its opening toward solution. The second hot spot was between Lys-314 and its symmetry mate and coincided roughly with the C site of the E2-SOS complex. Secondly, the polysaccharide appeared to follow the inner contour of the groove that connected the two hot spots. One end of the sugar probably extended out from the groove and lay on top of Arg-418 and Arg-414; the other end of the sugar extended toward the two-fold symmetry axis, but the details there remained unclear. The simultaneous binding of heparin to two protein protomers near the symmetry axis was expected to strengthen dimerization. Thirdly, the E2 domain contained four histidine residues (His-307, His-376, His-426, and His-433) that were absolutely conserved in evolution. The mapped footprint of heparin covered all four histidines. Among the four, His-376 made the largest contribution to heparin binding at neutral pH. At acidic pH, protonation of the histidines was expected to increase the affinity between the protein and heparin. The conservation of the histidines suggested that this property could have important functional consequences.

Inhibition of endogenous HS synthesis caused increased Aβ secretion from cells (33). Because the binding of HS to the E2 domain could affect APP in ways that might hinder its cleavage by β-secretase (for example, the HS-induced dimerization could cause clustering of the molecule or retain the precursor at sites where local HS concentrations were high; HS was known to inhibit β-secretase activity (33)), we wanted to determine whether the loss of E2-HS interaction could contribute to the observed increase in Aβ secretion. The mapping of the E2 heparin binding site allowed us to approach this problem from a different angle by specifically mutating APP residues that were involved in heparin binding. We tested three double mutants, which covered all major regions of the protein surface that heparin contacted. Based on our Western blot analysis, none of the three mutants caused any change in APP processing in cultured HEK-293 cells. Therefore, our result seemed to be in agreement with the hypothesis that endogenous HS influenced Aβ production primarily through its direct inhibition of β-secretase (33).

We could not yet explain the effects of the K476A/K477A double mutation. For the wild-type protein, the immature 100-kDa band corresponded to the *N*-glycosylated full-length APP (42). The surprising shift of this band to a higher molecular weight suggested that either the mutant protein migrated abnormally on SDS gel, which seemed very unlikely, or its post-translational modification (*e.g.* glycosylation) was altered. Whatever the change was, it apparently did not affect the addition of *O*-linked sugars to the protein, which increased the molecular mass by another 20 kDa (the upper mature band) (42). However, the proteolytic processing of the mutant protein by both α-secretases and β-secretases was greatly reduced. This reduction was probably unrelated to heparin binding because the two lysines (equivalent to Arg-414 and Arg-415 of APLP1) were located on the periphery of the heparin binding site, and other heparin binding site mutants did not have this effect. It was also intriguing that the single mutants (K476A, K477A) behaved just like the wild-type protein. Further studies of the double mutant are obviously required to address the unanswered questions. These studies may reveal new mechanisms that regulate APP processing in cells.

Acknowledgments—We thank S. Bian, D. Calderwood, and C. Chen for advice on mammalian cell culture. We also thank A. Heroux, H. Robinson, and A. Soares at NSLS X25 and X29 for assistance during x-ray diffraction data collection. Financial support for the beamlines comes principally from the United States Department of Energy and from the National Institutes of Health.

REFERENCES

1. Levy, E., Carman, M. D., Fernandez-Madrid, I. J., Power, M. D., Lieberburg, I., van Duinen, S. G., Bots, G. T., Luyendijk, W., and Frangione, B. (1990) *Science* **248,** 1124–1126
2. Goate, A., Chartier-Harlin, M. C., Mullan, M., Brown, J., Crawford, F., Fidani, L., Giuffra, L., Haynes, A., Irving, N., James, L., Mant, R., Newton, P., Rooke, K., Roques, P., Talbot, C., Pericak-Vance, M., Roses, A., Williamson, R., Rossor, M., Owen, M., and Hardy, J. (1991) *Nature* **349,** 704–706
3. Haass, C., Hung, A. Y., Selkoe, D. J., and Teplow, D. B. (1994) *J. Biol. Chem.* **269,** 17741–17748
4. Seubert, P., Vigo-Pelfrey, C., Esch, F., Lee, M., Dovey, H., Davis, D., Sinha, S., Schlossmacher, M., Whaley, J., Swindlehurst, C., *et al.* (1992) *Nature* **359,** 325–327
5. Glenner, G. G., and Wong, C. W. (1984) *Biochem. Biophys. Res. Commun.* **120,** 885–890
6. Hardy, J., and Selkoe, D. J. (2002) *Science* **297,** 353–356
7. Selkoe, D. J. (2001) *Physiol. Rev.* **81,** 741–766
8. Kang, J., Lemaire, H. G., Unterbeck, A., Salbaum, J. M., Masters, C. L.,

Grzeschik, K. H., Multhaup, G., Beyreuther, K., and Müller-Hill, B. (1987) *Nature* **325,** 733–736
9. Wasco, W., Bupp, K., Magendantz, M., Gusella, J. F., Tanzi, R. E., and Solomon, F. (1992) *Proc. Natl. Acad. Sci. U.S.A.* **89,** 10758–10762
10. Wasco, W., Gurubhagavatula, S., Paradis, M. D., Romano, D. M., Sisodia, S. S., Hyman, B. T., Neve, R. L., and Tanzi, R. E. (1993) *Nat. Genet.* **5,** 95–100
11. Zheng, H., Jiang, M., Trumbauer, M. E., Sirinathsinghji, D. J., Hopkins, R., Smith, D. W., Heavens, R. P., Dawson, G. R., Boyce, S., Conner, M. W., Stevens, K. A., Slunt, H. H., Sisoda, S. S., Chen, H. Y., and Van der Ploeg, L. H. (1995) *Cell* **81,** 525–531
12. von Koch, C. S., Zheng, H., Chen, H., Trumbauer, M., Thinakaran, G., van der Ploeg, L. H., Price, D. L., and Sisodia, S. S. (1997) *Neurobiol. Aging* **18,** 661–669
13. Heber, S., Herms, J., Gajic, V., Hainfellner, J., Aguzzi, A., Rülicke, T., von Kretzschmar, H., von Koch, C., Sisodia, S., Tremml, P., Lipp, H. P., Wolfer, D. P., and Müller, U. (2000) *J. Neurosci.* **20,** 7951–7963
14. Herms, J., Anliker, B., Heber, S., Ring, S., Fuhrmann, M., Kretzschmar, H., Sisodia, S., and Müller, U. (2004) *EMBO J.* **23,** 4106–4115
15. Wang, P., Yang, G., Mosier, D. R., Chang, P., Zaidi, T., Gong, Y. D., Zhao, N. M., Dominguez, B., Lee, K. F., Gan, W. B., and Zheng, H. (2005) *J. Neurosci.* **25,** 1219–1225
16. Storey, E., Beyreuther, K., and Masters, C. L. (1996) *Brain Res.* **735,** 217–231
17. Yamazaki, T., Koo, E. H., and Selkoe, D. J. (1997) *J. Neurosci.* **17,** 1004–1010
18. Sabo, S. L., Ikin, A. F., Buxbaum, J. D., and Greengard, P. (2001) *J. Cell Biol.* **153,** 1403–1414
19. Mok, S. S., Sberna, G., Heffernan, D., Cappai, R., Galatis, D., Clarris, H. J., Sawyer, W. H., Beyreuther, K., Masters, C. L., and Small, D. H. (1997) *FEBS Lett.* **415,** 303–307
20. Schubert, D., LaCorbiere, M., Saitoh, T., and Cole, G. (1989) *Proc. Natl. Acad. Sci. U.S.A.* **86,** 2066–2069
21. Ninomiya, H., Roch, J. M., Sundsmo, M. P., Otero, D. A., and Saitoh, T. (1993) *J. Cell Biol.* **121,** 879–886
22. Quast, T., Wehner, S., Kirfel, G., Jaeger, K., De Luca, M., and Herzog, V. (2003) *FASEB J.* **17,** 1739–1741
23. Gralle, M., Oliveira, C. L., Guerreiro, L. H., McKinstry, W. J., Galatis, D., Masters, C. L., Cappai, R., Parker, M. W., Ramos, C. H., Torriani, I., and Ferreira, S. T. (2006) *J. Mol. Biol.* **357,** 493–508
24. Gralle, M., Botelho, M. G., and Wouters, F. S. (2009) *J. Biol. Chem.* **284,** 15016–15025
25. Dahms, S. O., Hoefgen, S., Roeser, D., Schlott, B., Gührs, K. H., and Than, M. E. (2010) *Proc. Natl. Acad. Sci. U.S.A.* **107,** 5381–5386
26. Lee, S., Xue, Y., Hu, J., Wang, Y., Liu, X., Demeler, B., and Ha, Y. (2011) *Biochemistry* **50,** 5453–5464
27. Bergamaschini, L., Rossi, E., Storini, C., Pizzimenti, S., Distaso, M., Perego, C., De Luigi, A., Vergani, C., and De Simoni, M. G. (2004) *J. Neurosci.* **24,** 4181–4186
28. Kisilevsky, R., Lemieux, L. J., Fraser, P. E., Kong, X., Hultin, P. G., and Szarek, W. A. (1995) *Nat. Med.* **1,** 143–148
29. van Horssen, J., Wesseling, P., van den Heuvel, L. P., de Waal, R. M., and Verbeek, M. M. (2003) *Lancet Neurol.* **2,** 482–492
30. Leveugle, B., Ding, W., Durkin, J. T., Mistretta, S., Eisle, J., Matic, M., Siman, R., Greenberg, B. D., and Fillit, H. M. (1997) *Neurochem. Int.* **30,** 543–548
31. Leveugle, B., Ding, W., Laurence, F., Dehouck, M. P., Scanameo, A., Cecchelli, R., and Fillit, H. (1998) *J. Neurochem.* **70,** 736–744
32. Klaver, D., Hung, A. C., Gasperini, R., Foa, L., Aguilar, M. I., and Small, D. H. (2010) *Neurodegener. Dis.* **7,** 187–189
33. Scholefield, Z., Yates, E. A., Wayne, G., Amour, A., McDowell, W., and Turnbull, J. E. (2003) *J. Cell Biol.* **163,** 97–107
34. Hoopes, J. T., Liu, X., Xu, X., Demeler, B., Folta-Stogniew, E., Li, C., and Ha, Y. (2010) *J. Biol. Chem.* **285,** 2165–2173
35. Otwinowski, Z., and Minor, W. (1997) *Methods Enzymol.* **276,** 307–326
36. Brünger, A. T., Adams, P. D., Clore, G. M., DeLano, W. L., Gros, P., Grosse-Kunstleve, R. W., Jiang, J. S., Kuszewski, J., Nilges, M., Pannu, N. S., Read, R. J., Rice, L. M., Simonson, T., and Warren, G. L. (1998) *Acta Crystallogr D Biol. Crystallogr.* **54,** 905–921
37. Jones, T. A., Zou, J. Y., Cowan, S. W., and Kjeldgaard, M. (1991) *Acta Crystallogr. A* **47,** 110–119
38. Emsley, P., Lohkamp, B., Scott, W. G., and Cowtan, K. (2010) *Acta Crystallogr. D Biol. Crystallogr.* **66,** 486–501
39. Winn, M. D., Murshudov, G. N., and Papiz, M. Z. (2003) *Methods Enzymol.* **374,** 300–321
40. Parkash, V., Leppänen, V. M., Virtanen, H., Jurvansuu, J. M., Bespalov, M. M., Sidorova, Y. A., Runeberg-Roos, P., Saarma, M., and Goldman, A. (2008) *J. Biol. Chem.* **283,** 35164–35172
41. Wang, Y., and Ha, Y. (2004) *Mol. Cell* **15,** 343–353
42. Weidemann, A., König, G., Bunke, D., Fischer, P., Salbaum, J. M., Masters, C. L., and Beyreuther, K. (1989) *Cell* **57,** 115–126